analytical chemistry

pubs.acs.org/ac Article

Self-Enhanced Electrochemiluminesence of Dye-Doped Polymer Dots for Coreactant-Free Visualized Detection of Iodide Ions

Xuewei Cao,[#] Ziyu Wang,[#] Ben Liu, Xinyu Li, Shanshan Wu, Jingshuo Jiang, Jiankai Feng,* Huangxian Ju,* and Ningning Wang*

Cite This: *Anal. Chem.* 2024, 96, 17824−17830 Read Online

ACCESS | Metrics & More | Article Recommendations | Supporting Information

ABSTRACT: The monitoring of radioactive iodide levels is of great significance in environmental science and cancer radiotherapy. In this work, a high-throughput, radiation-resistant, and visualized electrochemiluminescence (ECL) strategy was developed for detection of iodide ions. Herein, the hydrophobic ruthenium derivative ($Ru(bpy)_3[B(C_6F_5)_4]_2$) (bpy = bipyridyl) was doped in tertiary amine-coupled polymer dots (N-PFO Pdots) to synthesize self-enhanced Pdots (Ru@Pdots), which showed extremely high ECL intensity in absence of coreactant. Due to the efficient ECL resonance energy transfer between $Ru(bpy)_3[B(C_6F_5)_4]_2$ and N-PFO, the Ru@Pdots exhibited 18 times higher ECL intensity compared with bare N-PFO Pdots. Besides, Ru@Pdots also showed 220-times higher ECL intensity compared with $Ru(bpy)_3[B(C_6F_5)_4]_2$ doped coreactant-dependent Pdots (Ru@PFO Pdots). Using Ru@Pdots as ECL emitters, an ECL imaging array was designed for iodide ion detection, which exhibited a detection range of 0.8 nM−4 μM and a limit of detection of 0.1 nM. In this strategy, iodide ions were oxidized as iodide free radicals on the surface of the electrode, which could further consume the nitrogen radical of Ru@Pdots and effectively quench the ECL signal. This method also showed good specificity, radiation-resistant performance, and accuracy in actual seawater sample testing, which indicated its value in marine environmental monitoring, nuclear security, and cancer radiotherapy.

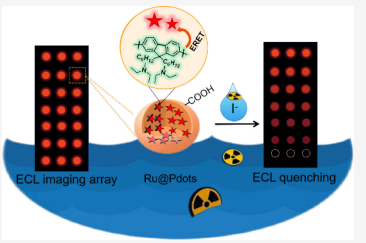

INTRODUCTION

Due to the rapid development of nuclear power technology and cancer radiation therapy, the amount of radioactive iodide (including $^{129}I^-$ and $^{131}I^-$) in natural water sources is gradually growing,[1,2] which causes extensive and irreversible damage to the global environment and public health.[3,4] These radioactive iodide isotopes can enter the ecosystem through air or water and gradually accumulate in the food chain to further influence the hyroid function and overall health of organisms, potentially increasing the risk of cancer.[5,6] Therefore, the development of rapid and accurate determination of iodide ions (the main chemical form of radioactive iodide in aqueous solution) in the environment has exhibited its significance in the field of environmental public security.[7] Currently reported methods for iodide detection include spectrophotometry,[8,9] electrochemical sensors,[10,11] fluorescence[12] and chemiluminescence[13] methods, etc. Restricted by the relatively low sensitivity and complex pretreatment steps, the accurate and convenient monitoring methods for iodide ions in actual water sources remains the significant concern in this field.

As a novel visual detection technique, electrochemiluminescence (ECL) imaging combines the advantages of bioimaging and ECL technology, which shows the advantages of high-throughput, high sensitivity, as well as the convenient detection process.[14−16] Owing to the superior spatiotemporal resolution and surface-confined sensitivity,[17,18] ECL imaging has been developed as a versatile surface analysis and multiplex targets analysis technology, which has been widely used in the field of exploration of ECL mechanism and bioanalysis.[19−21] ECL emitters play the crucial roles in the occurrence and development of ECL which enormously influence the sensitivity of ECL detection.[22−24] Polymer dots (Pdots) have attracted intense attention in the field of ECL, owing to the advantages of good biocompatibility, excellent photostability, and tunable optical and electrochemical properties.[25−27] The ECL behavior of Pdots can be easily adjusted through modification of the structures of monomer.[28,29] Our previous work introduced dual intramolecular electron transfer (DIET) to design a coreactant-embedded Pdots, which showed efficient ECL enhancing.[30] Whether the intramolecular and the intermolecular enhancement mechanisms can be combined to further enhance the ECL of Pdots attracts our considerable attentions.

Herein, self-enhanced Pdots were prepared by combining DIET and intermolecular resonance energy transfer (RET). The tertiary amine-coupled poly(9,9-dioctylfluorenyl-2,7-diyl) polymer (N-PFO) was first synthesized and served as carrier

Received: August 13, 2024
Revised: October 7, 2024
Accepted: October 15, 2024
Published: October 22, 2024

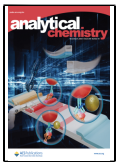

Scheme 1. (A) Preparation Diagram of Ru@Pdots and (B) Schematic Diagrams of ECL Imaging Detection for I^-

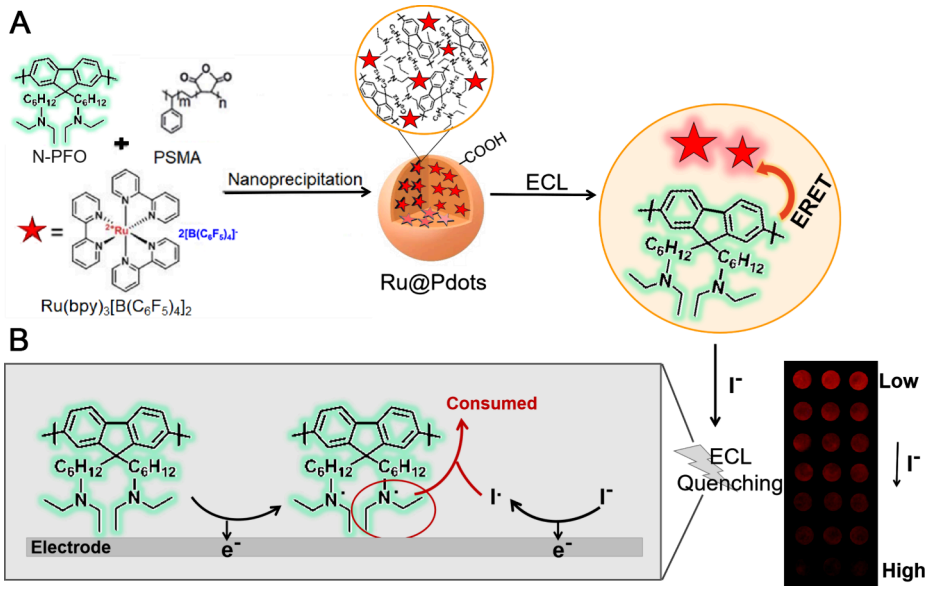

for encapsulating the derivatives of tris(bipyridyl)ruthenium-(II) complexes ($Ru(bpy)_3[B(C_6F_5)_4]_2$), to prepare the dye-doped Pdots (Ru@Pdots, Scheme 1A). Thanks to the DIET of N-PFO Pdots and the efficient RET of $Ru(bpy)_3[B(C_6F_5)_4]_2$ and N-PFO, the Ru@Pdots exhibited 18-times higher ECL compared with bare N-PFO Pdots and 220-times higher ECL intensity than $Ru(bpy)_3[B(C_6F_5)_4]_2$ doped coreactant-dependent Pdots (Ru@PFO Pdots). Utilizing this Ru@Pdots as a self-enhanced ECL probe, an ECL imaging array was proposed for visual detection of iodide ions. Specifically, I^- was oxidized to iodide radical ions on the electrode surface, which caused the consumption of nitrogen radicals on the N-PFO side chains and thus quenched the ECL of Ru@Pdots (Scheme 1B). This strategy offers a wide detection range, radiation-resistant feature, and high sensitivity for iodide ion detection, which also enabled the visualization of iodide content in natural seawater samples. The analytical performance of this strategy demonstrated its good accuracy for iodide ion detection, providing a practical avenue in several fields, such as marine environmental monitoring, nuclear radiation pollution, biological health, etc.

EXPERIMENTAL SECTION

Materials, Reagents, and Apparatus. The detailed information is described in the Supporting Information.

Synthesis of N-PFO. The tertiary amine-coupled polymer (N-PFO) was synthesized according to Figure S1. For the synthesis of M3, M1 (0.150 g, 0.23 mmol), M2 (0.13 g, 0.23 mmol), and $Pd(PPh_3)_4$ (0.030 g, 5% eq) were dissolved in 20 mL of toluene and K_2CO_3 (1.30 g) in water (5 mL). The mixture was refluxed for 48 h under an Ar atmosphere. The organic phase was dried with Na_2SO_4, and the solvent was removed. The resulting mixture was then dissolved in 2 mL of tetrahydrofuran (THF) and dropped into 300 mL of hexane to give M3 as a bright yellow solid (0.13 g, 72.2%). ^{1}H NMR (400 MHz, Chloroform-*d*) δ 7.87−7.85 (m, 2H), 7.71−7.65 (m, 4H), 4.18−3.02 (m, 4H), 2.41−2.06 (m, 3H), 2.03−1.88 (m, 3H), 1.73−1.67 (m, 1H), 1.50−1.40 (m, 2H), 1.28−1.26 (m, 3H), 1.19 (s, 4H), 1.00−0.56 (m, 4H). For the synthesis of N-PFO, M3 (0.13 g) was added into 5 mL of diethylamide, 20 mL of THF, and 5 mL of DMF with 0.1 g of K_2CO_3. The mixture was refluxed under an Ar atmosphere for 4 d, the solvent was removed, and the residue was dissolved in 2 mL of THF and dropped into 300 mL of hexane; the solid conjugated polymer was filtered as the product (0.10 g). ^{1}H NMR (400 MHz, Chloroform-*d*) δ 7.86−7.49 (m, 6H), 3.97−3.92 (m, 1.2H), 3.49 (s, 0.9H), 2.64−0.55 (m, 31.4H). GPC data: Mw = 41107, Mn = 17242, PDI = 2.38.

Synthesis of $Ru(bpy)_3[B(C_6F_5)_4]_2$. $Ru(bpy)_3[B(C_6F_5)_4]_2$, a ruthenium derivative, was synthesized through a metathesis reaction.[31] Briefly, the aqueous solution of $Ru(bpy)_3Cl_2{\cdot}6H_2O$ (74.9 mg, 0.1 mmol) was added dropwise into the solution of $Li[B(C_6F5)_4]_2{\cdot}nEt_2O$ (217.2 mg, 0.1 mmol) and gradually mixed at room temperature under constant stirring for 1 h (Figure S2). The resulting orange-red precipitate was washed three times with water through centrifugation. Then, the precipitate was dried overnight at 80 °C and recrystallized to obtain the hydrophobic $Ru(bpy)_3[B(C_6F_5)_4]_2$. ^{1}H NMR (400 MHz, THF-d_8) δ 8.57 (dt, J = 8.2, 1.1 Hz, 6H), 8.01 (td, J = 7.9, 1.5 Hz, 6H), 7.73−7.67 (m, 6H), 7.33 (ddd, J = 7.2, 5.6, 1.3 Hz, 6H).

Preparation of Ru@Pdots. N-PFO, PSMA, and $Ru(bpy)_3[B(C_6F_5)_4]_2$ were separately dissolved in THF at a concentration of 10 mg/mL. Then, 100 μL of N-PFO, 200 μL of $Ru(bpy)_3[B(C_6F_5)_4]_2$, 50 μL of PSMA, and 9.65 mL of tetrahydrofuran (THF) were mixed to get the precursor solution. After it was degassed via ultrasonication for 5 min, the precursor solution was rapidly injected into 90 mL of ultrapure water in a bath sonicator and kept for 3 min. The solution was concentrated through rotary evaporation to obtain the final $Ru(bpy)_3[B(C_6F_5)_4]_2$ dropped N-PFO Pdots (Ru@Pdots, 50 μg/mL).

ECL Detection of Iodide Ion. For normal I^- detection, Ru@Pdots (50 μg/mL, 6 μL) were modified on a glassy carbon electrode (GCE). The GCEs were inset into 0.1 M PBS pH 7.4. For ECL imaging detection, Ru@Pdots (50 μg/mL, 2.5 μL) were separately modified in the array of carbon-coated ITO (C/ITO). After these modified Pdots were dried at 37 °C for 30 min, a constant potential of 1.2 V was applied on C/ITO for 10 s. The ECL images were acquired by a self-made

https://doi.org/10.1021/acs.analchem.4c04301
Anal. Chem. 2024, 96, 17824−17830

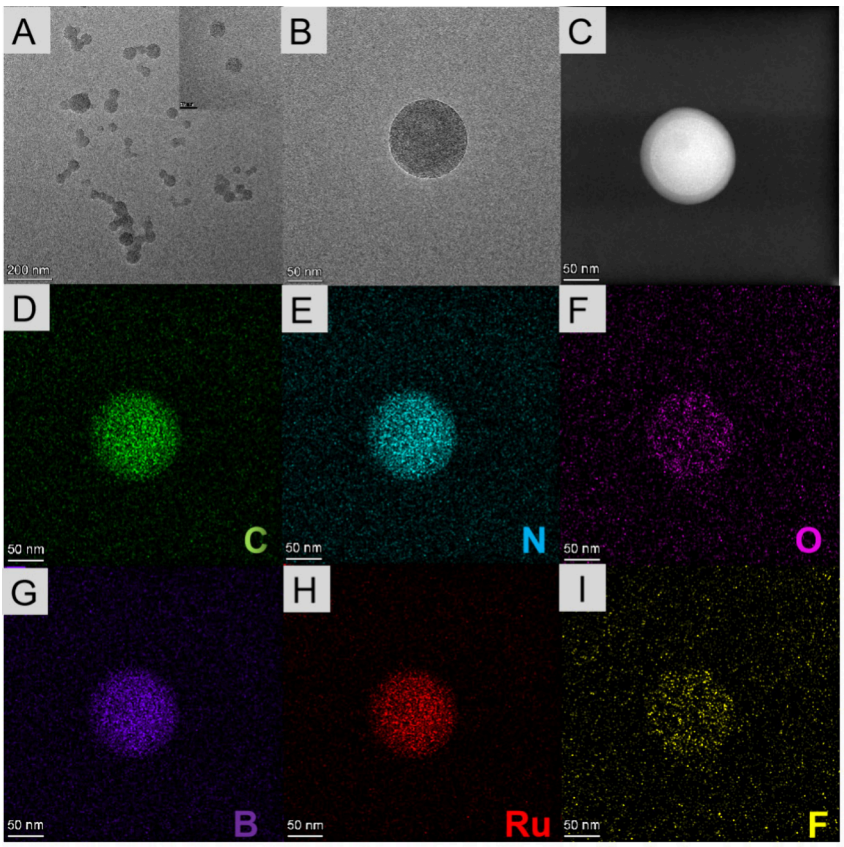

Figure 1. (A) TEM image of Ru@Pdots. (B) High-resolution TEM image of a single Ru@Pdots. (C) HAADF image of Ru@Pdots with the mapped region of different elements (D) C, (E) N, (F) O, (G) B, (H) Ru, and (I) F.

ECL imaging system, which included a color camera (UOP0600CSC, China UOP) and a lens (Canon 50, EF 1.2).

Radiation Resistance Test. First, Ru@Pdots was immobilized on polished and cleaned glassy carbon electrodes, which were then divided into two groups. One group was placed in a glass container (0.7 L) containing 0.3 MBq of ^{131}I for radiation treatment as the experimental group. The other group was placed in a glass container (0.7 L) without I-131 as the control group. After 30 min, ECL signals of both groups were independently detected in 0.1 M PBS pH 7.4.

Seawater Treatment. The collected seawater sample was first allowed to settle, and we removed the sediments. Then, filter paper was utilized to remove macromolecular impurities from the seawater. Subsequently, the simply filtered seawater was further purified through a 0.22 μm membrane. The obtained seawater solution was then stored in clean centrifuge tubes at 4 °C.

RESULTS AND DISCUSSION

Characterization of Ru@Pdots. N-PFO polymer was prepared through a nucleophilic substitution reaction (Figure S1). And $Ru(bpy)_3[B(C_6F_5)_4]_2$ was synthesized through a metathesis reaction (Figure S2). The $Ru(bpy)_3[B(C_6F_5)_4]_2$ exhibited a distinct absorption peak at 450 nm and a fluorescence emission peak at around 605 nm, which were essentially consistent with the peaks of commercialized $Ru(bpy)_3^{2+}$ in aqueous solution (Figure S3), confirming the successful preparation of $Ru(bpy)_3[B(C_6F_5)_4]_2$. The Ru@Pdots were prepared by co-nanoprecipitation of $Ru(bpy)_3[B(C_6F_5)_4]_2$, PSMA, and N-PFO polymer (Scheme 1A). As exhibited in Figure S4, Ru@Pdots showed three absorption peaks at 288, 390, and 455 nm, which were attributed to the absorption peaks merge of N-PFO Pdots and $Ru(bpy)_3[B(C_6F_5)_4]_2$, and confirmed the successful doping of $Ru(bpy)_3[B(C_6F_5)_4]_2$ in Pdots. Besides, the transmission electron microscopy (TEM) image showed that the Ru@Pdots were spherical particles with a diameter of approximately 100 nm (Figure 1A,B). The high-angle annular dark field (HAADF) image (Figure 1C) and energy-dispersive X-ray spectroscopy (EDS) (Figure 1D-I) exhibited a clear distribution of elements C, N, O, B, Ru, and F, which further confirmed the effective doping of $Ru(bpy)_3[B(C_6F_5)_4]_2$ in Ru@Pdots.

ECL-RET of Ru@Pdots. The fluorescence emission spectrum of N-PFO Pdots showed a significant overlap with the excitation spectrum of $Ru(bpy)_3[B(C_6F_5)_4]_2$ between 405 and 530 nm (Figure S5), which implied the feasibility of RET between $Ru(bpy)_3[B(C_6F_5)_4]_2$ and N-PFO Pdots. To obtain optimal ECL performance, the doping amounts of $Ru(bpy)_3[B(C_6F_5)_4]_2$ and PSMA in Ru@Pdots were separately investigated. As shown in Figure 2A, the ECL intensity increased with the increasing amount of $Ru(bpy)_3[B(C_6F_5)_4]_2$, which reached the maximum value at the ratio of 2 (Ru/N-PFO, w/w) with a slight decrease at 3, attributed to the increase of receptor of RET leading to more efficient RET, while too many hydrophobic $Ru(bpy)_3[B(C_6F_5)_4]_2$ resulted in the reduced ECL. The amount of PSMA could also influence the ECL response of Ru@Pdots, because it provided the hydrophilic carboxyl group, which was beneficial for electrochemical reactions.[32,33] As shown in Figure 2B, the Ru@Pdots exhibited the strongest ECL emission at a ratio of 0.5 (PSMA/

https://doi.org/10.1021/acs.analchem.4c04301
Anal. Chem. 2024, 96, 17824−17830

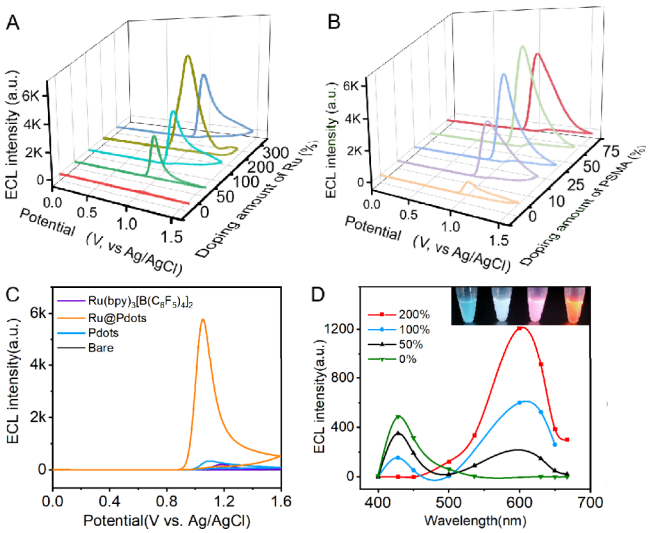

Figure 2. (A) ECL curves of Ru@Pdots prepared with different doping ratios of $Ru(bpy)_3[B(C_6F_5)_4]_2$. (B) ECL curves of Ru@Pdots prepared with different concentrations of PSMA. (C) ECL curves of 50 μg/mL N-PFO Pdots, 50 μg/mL Ru@Pdots, and 100 μg/mL $Ru(bpy)_3[B(C_6F_5)_4]_2$ modified GCEs in PBS. (D) ECL spectra of Ru@Pdots with different amounts of $Ru(bpy)_3[B(C_6F_5)_4]_2$. Inset: Photo of Ru@Pdots under 365 nm UV light.

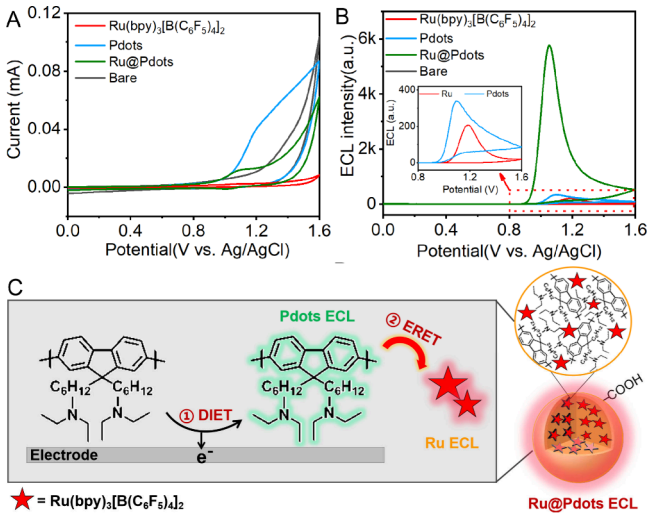

Figure 3. (A) CV and (B) ECL curves of $Ru(bpy)_3[B(C_6F_5)_4]_2$, N-PFO Pdots, Ru@Pdots, and bare GCE in 0.1 M PBS containing 0.1 M KNO_3. Inset: magnified ECL curves. (C) ECL-RET mechanism of Ru@Pdots.

N-PFO, w/w). Under the optimum conditions, Ru@Pdots exhibited 28-fold and 17-fold higher ECL than the equivalent amounts of N-PFO Pdots and $Ru(bpy)_3[B(C_6F_5)_4]_2$ (Figure 2C), which suggested the ECL-RET effect between N-PFO Pdots and $Ru(bpy)_3[B(C_6F_5)_4]_2$ greatly enhanced the ECL of final Ru@Pdots.

Additionally, the fluorescence and ECL spectra of Ru@Pdots with different amounts of $Ru(bpy)_3[B(C_6F_5)_4]_2$ were studied to explore its ECL-RET. As shown in Figure 2D and Figure S6, when $Ru(bpy)_3[B(C_6F_5)_4]_2$ was absent, the Pdots only exhibited emission peaks of N-PFO at 425 and 460 nm. With increasing of $Ru(bpy)_3[B(C_6F_5)_4]_2$, the intensity of N-PFO emission peaks decreased, which accompanied by the emergence and increasing of emission peaks of $Ru(bpy)_3[B(C_6F_5)_4]_2$ at 600 nm. While the doping amount reached 200%, the emission peak of Ru@Pdots completely exhibited the emission of the receptor $Ru(bpy)_3[B(C_6F_5)_4]_2$ rather than the donor N-PFO, which confirmed that the ECL-RET reached its maximum. This phenomenon sufficiently demonstrated that the ECL-RET mechanism happened between N-PFO and $Ru(bpy)_3[B(C_6F_5)_4]_2$.

Electrochemical and ECL Behaviors of Ru@Pdots. The ECL mechanism of Ru@Pdots was investigated by comparing the electrochemical and ECL behaviors of $Ru(bpy)_3[B(C_6F_5)_4]_2$, N-PFO Pdots, and Ru@Pdots modified glassy carbon electrodes (GCEs) in 0.1 M PBS (pH 7.4). As shown in Figure 3A, $Ru(bpy)_3[B(C_6F_5)_4]_2$ exhibited negligible electrochemical oxidation currents in PBS owing to its hydrophobicity. The Ru@Pdots showed an obvious oxidation peak at +1.1 V with the onset potential of +0.7 V, which was close to the onset potential of N-PFO Pdots. As shown in Figure 3B, $Ru(bpy)_3[B(C_6F_5)_4]_2$ exhibited a weak ECL peak at +1.2V with the onset potential of +1.0 V. The Ru@Pdots showed an ECL emission peak at +1.0 V and an onset potential of +0.9 V, which were both consistent with N-PFO Pdots. This phenomenon implied the ECL of Ru@Pdots generated with the oxidation of N-PFO was more positive than that of $Ru(bpy)_3[B(C_6F_5)_4]_2$. The 18-times enhanced ECL of Ru@Pdots compared with N-PFO Pdots owing to the efficient ECL-RET. Figure 3C provides a detailed description of this ECL mechanism of Ru@Pdots: the tertiary amine groups on the side chains of N-PFO were first oxidized on the electrode and resulted in ECL emission of N-PFO Pdots through DIET.[30] Subsequently, the ECL of N-PFO excited the emission of $Ru(bpy)_3[B(C_6F_5)_4]_2$ to further produce the extremely increased ECL signal through ECL-RET.[34,35]

Moreover, the ECL performance of Ru@Pdots was compared with $Ru(bpy)_3[B(C_6F_5)_4]_2$ doped PFO Pdots (Ru-PFO Pdots), which did not contain the DIET process. The concentration of N-PFO in 50 μg mL^{-1} Ru@Pdots was around 100 μM, and the corresponding theoretical concentration of tertiary amine was 200 μM. The ECL of 50 μg mL^{-1} Ru@Pdots in PBS was around 220 times higher than that of Ru@PFO Pdots in 400 μM TEA (Figure 4A), which implied the more significant ECL-RET effect in Ru@Pdots. To support this point, we recorded fluorescence spectra and time-resolved fluorescence measurements of Ru@Pdots and Ru@PFO Pdots. As shown in Figure 4B, Ru@PFO Pdots exhibited strong PFO emission peaks at 425 nm and 460 nm and a weaker peak at 600 nm, which indicated the incomplete RET between PFO and $Ru(bpy)_3[B(C_6F_5)_4]_2$. In contrast, the Ru@Pdots showed a strong emission peak at 600 nm, with negligible peaks at 425 and 460 nm, which proved the complete RET between N-PFO and $Ru(bpy)_3[B(C_6F_5)_4]_2$. Time-resolved fluorescence lifetimes were also used to analyze the RET process of Ru@PFO Pdots and Ru@Pdots. For comparison, the average lifetime of Ru@PFO Pdots at 600 nm was 10.5 ns (Figure 4C), which was much shorter than that of Ru@Pdots (3.8 μs, Figure 4D). This result also suggested that more effective RET occurred between N-PFO and $Ru(bpy)_3[B(C_6F_5)_4]_2$ in the Ru@Pdots, due to the possible interaction of N and Ru,[36,37] which narrowed the distance between the donor and receptor, leading to a more significant RET effect.

Iodide Ion Detection. The prepared Ru@N-PFO Pdots at the optimal doping ratio were utilized as detection probes for the ECL detection of iodide ions. The ECL intensity of Ru@Pdots gradually decreased (Figure 5A) with the increased

https://doi.org/10.1021/acs.analchem.4c04301
Anal. Chem. 2024, 96, 17824−17830

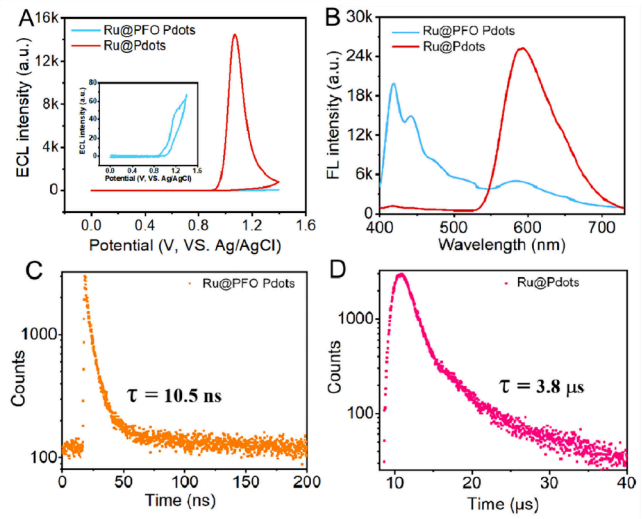

Figure 4. (A) ECL curves of 50 μg/mL Ru@Pdots modified GCE in 0.1 M PBS and 50 μg/mL Ru@PFO Pdots modified GCE in 0.1 M PBS containing 200 μM TEA. (B) Fluorescence spectra of Ru@Pdots and Ru@PFO Pdots. Fluorescence lifetimes of (C) Ru@PFO Pdots and (D) Ru@Pdots. λ_{ex} = 375 nm; λ_{em} = 600 nm.

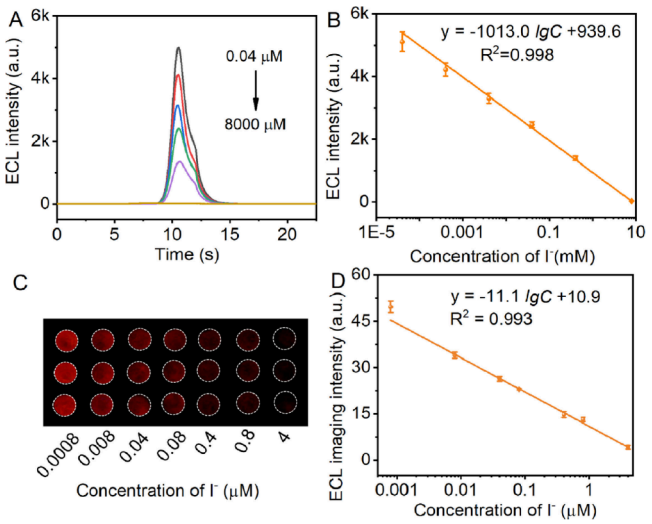

Figure 5. (A) ECL curves and (B) the calibration curve for detection of different concentrations of I^- from 40 nM to 8 mM. (C) ECL image and (D) the calibration curve for visual detection of different concentrations of I^- from 0.8 nM to 4 μM (n = 3).

iodide ions concentration, which was attributed to the quenching effect of iodide ions on the anode ECL of Ru@N-PFO Pdots. Specifically, we attribute this to the oxidation of iodide ions to iodide radicals, which could further react with nitrogen radicals generated from the tertiary amines on the N-PFO side chains via an annihilation pathway.[38] As a result, the DIET process of N-PFO Pdots was inhibited, which thereby quenched the ECL signal of Ru@Pdots. Within the range from 40 nM to 8 mM, a good linear relationship between the logarithm of the ECL intensity and the concentration of iodide ions was observed, with a detection limit (LOD) of 5 nM (Figure 5B). Based on the high ECL signal intensity of Ru@Pdots, we further investigated its application in ECL imaging detection of iodide ions, by introducing the imaging array to design the multiple targets analysis strategy.[39] The results revealed that the imaging brightness of Ru@Pdots in the ECL imaging array also decreased with the increase in the iodide ion concentration (Figure 5C). Meanwhile, the logarithm of the ECL imaging intensity also showed a good linear relationship with the concentration of iodide ions (Figure 5D), which showed a lower LOD of 0.1 nM, and a wide detection range from 0.8 nM to 4 μM. These results indicated that the ECL imaging detection of iodide ion based on Ru@Pdots had significant implications for the development of fast, sensitive, and high-throughput visual monitoring of iodide ions.

Performance Evaluation of the Strategy. To explore the specificity of the strategy, the ECL intensities of Ru@Pdots in different solutions were compared. As shown in Figure 6A,

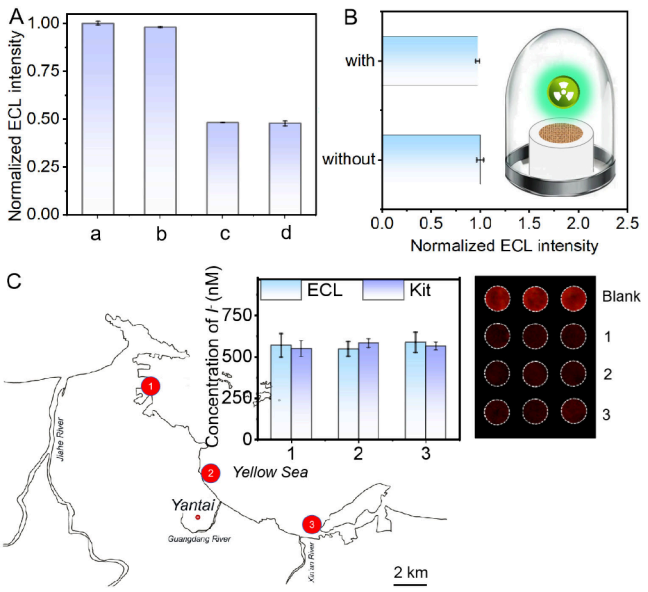

Figure 6. (A) Normalized ECL intensity of Ru@Pdots modified GCEs in the presence of blank (a), interfering ions (b), 80 μM I^- (c), and 80 μM I^- + interfering ions (d). Interfering ions: Cl^-, Br^-, NO_3^-, SO_4^{2-}, CO_3^{2-}, HCO_3^-, $H_2PO_4^-$, and HPO_4^{2-} at 80 μM. (B) Normalized ECL intensity of Ru@Pdots modified GCEs under radiative and nonradiative conditions. (C) ECL images and the comparison of the proposed ECL method with commercial kits for I^- detection in seawater samples from three locations.

the ECL of Ru@Pdots in interfering ions (80 μM Cl^-, Br^-, NO_3^-, SO_4^{2-}, CO_3^{2-}, HCO_3^-, $H_2PO_4^-$, and HPO_4^{2-}) was basically consistent with that in the blank solution. But there was a significant ECL quenching effect while the solution contained 80 μM I^-, and the ECL of Ru@Pdots in 80 μM I^- was the same as the mixture of interfering ions with 80 μM I^-. That demonstrated the high specificity of this ECL sensing strategy, providing the possibility for rapid and accurate detection of iodide in a complex environment.

To meet the increasingly complex demands of environmental changes, irradiation treatments of Ru@Pdots were conducted. After the Ru@Pdots modified GCEs were exposed to the radioactive ^{131}I environment for 30 min, the ECL signal of the experimental group showed no significant change compared to the control group, demonstrating the significance of this method for monitoring radioactive environments (Figure 6B).

Besides, the iodide ion contents in seawater samples were further analyzed by collecting seawater from three locations near Yan Tai City (121°E, 37°N). The detection results obtained by this method were essentially consistent with those

https://doi.org/10.1021/acs.analchem.4c04301
Anal. Chem. 2024, 96, 17824−17830

from commercial assay kits (Figure 6C), which implied accuracy of the analysis. The Ru@Pdots also exhibited good ECL stability for iodide ion detection over a two-week period (Figure S7). These results demonstrated the excellent performances of this strategy in high sensitivity, good specificity, excellent radiation resistance, and good stability, which also indicated the potential of the proposed ECL strategy for rapid, sensitive, and high-throughput detection of iodide ions in complex environments.

CONCLUSION

This work designs novel self-enhanced doped-type Pdots based on the combination of DIET and RET mechanism, which exhibits strong ECL emission in PBS. The ECL mechanism was explored and confirmed to explain its high ECL intensity, and then developed Pdots were successfully utilized for ECL imaging detection of iodide ions, with a detection limit as low as 0.1 nM. This method offers advantages such as wide detection range, high sensitivity, and good selectivity. Furthermore, it is unaffected by radioactive environments and demonstrates good detection accuracy when applied to actual seawater samples. The proposed strategy provides a new tool for the visual detection of radioactive iodide in marine environments and the rapid detection of iodide ions in nuclear safety.

ASSOCIATED CONTENT

Supporting Information

The Supporting Information is available free of charge at https://pubs.acs.org/doi/10.1021/acs.analchem.4c04301.

Materials, reagents and apparatus, Synthetic route of polymer N-PFO and $Ru(bpy)_3[B(C_6F_5)_4]_2$, UV−vis absorption and FL spectra of $Ru(bpy)_3[B(C_6F_5)_4]_2$ and $Ru(bpy)_3^{2+}$, UV−vis absorption spectra of N-PFO Pdots, Ru@Pdots and $Ru(bpy)_3[B(C_6F_5)_4]_2$, EDS spectrum and atomic percentages of Ru@Pdots, ECL stability of Ru@Pdots|GCE, ^1H NMR of M3, N-PFO and $Ru(bpy)_3[B(C_6F_5)_4]_2$ (PDF)

AUTHOR INFORMATION

Corresponding Authors

Jiankai Feng − *Yantai Affiliated Hospital of Binzhou Medical University, Yantai 264100, China*; Email: 15154502685@163.com

Huangxian Ju − *State Key Laboratory of Analytical Chemistry for Life Science, School of Chemistry and Chemical Engineering, Nanjing University, Nanjing 210093, P.R. China*; orcid.org/0000-0002-6741-5302; Email: hxju@nju.edu.cn

Ningning Wang − *School of Pharmacy, Binzhou Medical University, Yantai 264003, China*; orcid.org/0009-0009-3114-8394; Email: nnw@bzmc.edu.cn

Authors

Xuewei Cao − *School of Pharmacy, Binzhou Medical University, Yantai 264003, China; Qilu Medical University, Zibo 255300, P.R. China; Yantai Affiliated Hospital of Binzhou Medical University, Yantai 264100, China*

Ziyu Wang − *State Key Laboratory of Radiation Medicine and Protection, School for Radiological and Interdisciplinary Sciences, Soochow University, Suzhou 215123, P.R. China*; orcid.org/0000-0001-7832-3334

Ben Liu − *Yantai Affiliated Hospital of Binzhou Medical University, Yantai 264100, China*

Xinyu Li − *School of Pharmacy, Binzhou Medical University, Yantai 264003, China*

Shanshan Wu − *School of Pharmacy, Binzhou Medical University, Yantai 264003, China*

Jingshuo Jiang − *School of Pharmacy, Binzhou Medical University, Yantai 264003, China*

Complete contact information is available at: https://pubs.acs.org/10.1021/acs.analchem.4c04301

Author Contributions

#(X.C. and Z.W.) These authors contributed equally to this work.

Notes

The authors declare no competing financial interest.

ACKNOWLEDGMENTS

We acknowledge the financial support of the Natural Science Foundation of Shandong Province (ZR2022QB033), National Natural Science Foundation of China (22304015), the Scientific Research Start-up Fund of Binzhou Medical University (BY2022KYQD43), State Key Laboratory of Analytical Chemistry for Life Science (SKLACLS2403).

REFERENCES

(1) Chang, Y. C.; Zhao, X.; Jian, A.; Tan, Y. *Mar. Pollut. Bull.* **2024**, *198*, No. 115853.

(2) Rose, P. S.; Smith, J. P.; Aller, R. C.; Cochran, J. K.; Swanson, R. L.; Coffin, R. B. *Environ. Sci. Technol.* **2015**, *49*, 10312−10319.

(3) Taylor, D.; Dalgarno, S. J.; Xu, Z.; Vilela, F. *Chem. Soc. Rev.* **2020**, *49*, 3981−4042.

(4) Steinhauser, G. *Environ. Sci. Technol.* **2014**, *48*, 4649−4663.

(5) Zhou, X. Y.; Mao, P.; Jin, H. R.; Huang, W. X.; Gu, A. T.; Chen, K. W.; Yun, S.; Chen, J.; Yang, Y. *J. Hazard. Mater.* **2023**, *443*, No. 130349.

(6) Kupper, F. C.; Feiters, M. C.; Olofsson, B.; Kaiho, T.; Yanagida, S.; Zimmermann, M. B.; Carpenter, L. J.; Luther, G. R.; Lu, Z.; Jonsson, M.; et al. *Angew. Chem., Int. Ed. Engl.* **2011**, *50*, 11598−11620.

(7) Zhao, Q.; Liu, R. X.; Wang, Z. R.; Chen, G. Y.; Duan, T.; Zhu, L. *Environ. Sci.:nano* **2024**, *11*, 149−160.

(8) Chen, L.; Lu, W. H.; Wang, X. K.; Chen, L. X. *Sensor. Actua. B-Chem.* **2013**, *182*, 482−488.

(9) Yang, X. H.; Ling, J.; Peng, J.; Cao, Q. E.; Ding, Z. T.; Bian, L. C. *Anal. Chim. Acta* **2013**, *798*, 74−81.

(10) Khunseeraksa, V.; Kongkaew, S.; Thavarungkul, P.; Kanatharana, P.; Limbut, W. *Microchim. Acta* **2020**, *187*, 591.

(11) Chen, S. H.; Song, N.; Zhong, M. X.; Wang, C.; Lu, X. F. *Anal. Chim. Acta* **2021**, *1144*, 122−129.

(12) Zhang, Y. F.; He, Z. J.; Shen, X. Y.; Zhu, L. L.; Wang, D. Q.; Chen, Y. L.; Zhou, M. *Acs Appl. Polym. Mater.* **2023**, *5*, 2877−2886.

(13) Li, T.; Liang, G.; Li, X. H. *The Analyst* **2013**, *138*, 1898−1902.

(14) Liu, Y. H.; Guo, W. L.; Su, B. *Chin. Chem. Lett.* **2019**, *30*, 1593−1599.

(15) Chen, M. M.; Xu, C. H.; Zhao, W.; Chen, H. Y.; Xu, J. J. *Angew. Chem., Int. Ed.* **2022**, *61*, No. e202117401.

(16) Liu, Y. J.; Zhang, H. D.; Li, B.; Liu, J. W.; Jiang, D. C.; Liu, B. H.; Sojic, N. *J. Am. Chem. Soc.* **2021**, *143*, 17910−17914.

(17) Guo, W. L.; Zhou, P.; Sun, L.; Ding, H.; Su, B. *Angew. Chem., Int. Ed.* **2021**, *60*, 2089−2093.

(18) Voci, S.; Goudeau, B.; Valenti, G.; Lesch, A.; Jovic, M.; Rapino, S.; Paolucci, F.; Arbault, S.; Sojic, N. *J. Am. Chem. Soc.* **2018**, *140*, 14753−14760.

(19) Li, L. L.; Chen, W. W.; Hu, X. F.; Tang, Z. W.; Wang, C.; Ju, H. X. *Anal. Chem.* **2024**, *96*, 4308−4313.

(20) Knežević, S.; Han, D. N.; Liu, B. H.; Jiang, D. C.; Sojic, N. *Angew. Chem., Int. Ed.* **2024**, *63*, No. e202407588.
(21) Han, S.; Lee, H. J.; Kim, T.; Lim, S. Y.; Kim, J. *Anal. Chem.* **2024**, *96*, 11146−11154.
(22) Luo, R. G.; Luo, X.; Xu, H. C.; Wan, S. S.; Lv, H. F.; Zou, B. E.; Wang, Y. F.; Liu, T. R.; Wu, C.; Chen, Q. Z.; Yu, S. Q.; Dong, P. F.; Tian, Y. X.; Xi, K.; Yuan, S.; Wu, X. J.; Ju, H. X.; lei, J. P. *J. Am. Chem. Soc.* **2024**, *146* (24), 16681−16688.
(23) Ai, Y. J.; Gao, X. W.; Ren, X. X.; Li, M. W.; Zhang, B.; Zou, G. Z. *Anal. Chem.* **2024**, *96*, 6652−6658.
(24) Du, D. X.; Shu, J. N.; Guo, M. Q.; Haghighatbin, M. A.; Yang, D.; Bian, Z. P.; Cui, H. *Anal. Chem.* **2020**, *92*, 14113−14121.
(25) Feng, Y. Q.; Wang, N. N.; Ju, H. X. *Sci. China Chem.* **2022**, *65*, 2417−2436.
(26) Luo, J. H.; Li, Q.; Chen, S. H.; Yuan, R. *Acs Appl. Mater. Interfaces* **2019**, *11*, 27363−27370.
(27) Xiang, S.; Li, J. X.; Wang, F. T.; Yang, Y.; Yang, H. F.; Cai, R.; Tan, W. H. *Acs Appl. Mater. Interfaces* **2024**, *16*, 37748−37756.
(28) Gao, H.; Shi, S. Y.; Wang, S. M.; Tao, Q. Q.; Ma, H. L.; Hu, J.; Chen, H. Y.; Xu, J. J. *Aggregate* **2024**, *5*, No. e394.
(29) Mao, Z. W.; Dai, C. J.; Xu, Y. Y.; Jia, J. L.; Ke, L. B.; Zhou, Y. Y. *Anal. Chem.* **2024**, *96*, 12760−12766.
(30) Wang, N. N.; Gao, H.; Li, Y. Z.; Li, G. M.; Chen, W. W.; Jin, Z. C.; Lei, J. P.; Wei, Q.; Ju, H. X. *Angew. Chem., Int. Ed.* **2021**, *60*, 197−201.
(31) Feng, Y. Q.; Sun, F.; Wang, N. N.; Lei, J. P.; Ju, H. X. *Anal. Chem.* **2017**, *89*, 7659−7666.
(32) Gao, H.; Zhang, N.; Hu, J.; Pan, J. B.; Cheng, Y. X.; Chen, H. Y.; Xu, J. J. *Acs Appl. Nano Mater.* **2021**, *4*, 7244−7252.
(33) Luo, J. H.; Cheng, D.; Li, P. X.; Yao, Y.; Chen, S. H.; Yuan, R.; Xu, W. J. *Chem. Commun.* **2018**, *54*, 2777−2780.
(34) Wang, N. N.; Wang, Z. Y.; Chen, L. Z.; Chen, W. W.; Quan, Y. W.; Cheng, Y.; Ju, H. X. *Chem. Sci.* **2019**, *10*, 6815−6820.
(35) Lai, W. J.; Li, J. J.; Jiang, M. Z.; Li, P. L.; Wang, M.; Ma, C. Y.; Zhao, C. L.; Qi, Y.; Hong, C. L. *Anal. Chem.* **2023**, *95*, 7109−7117.
(36) Ban, C.; Yang, S.; Kim, H.; Kim, D. H. *Catal. Today* **2020**, *352*, 66−72.
(37) Chen, J. L.; Zhu, Z. H.; Wang, S. B.; Ma, Q.; Rudolph, V.; Lu, G. Q. *Chem. Eng. J.* **2010**, *156*, 404−410.
(38) Wang, Z. Y.; Zhao, Z.; Pei, Y.; Xia, Y.; Chen, F. L.; Xu, M. Y.; Gao, H.; Hua, D. B. *Sens. Actuators B Chem.* **2023**, *395*, No. 134506.
(39) Zhan, J. Z.; Shi, F.; Li, J.; Zeng, H.; Chen, M.; Hu, X. Y.; Yang, Z. J. *Chin. Chem. Lett.* **2023**, *34*, No. 108791.

https://doi.org/10.1021/acs.analchem.4c04301
Anal. Chem. 2024, 96, 17824−17830